

---

# Deep Sets

---

Manzil Zaheer<sup>1,2</sup> Satwik Kottur<sup>2</sup> Siamak Ravanbakhsh<sup>2</sup> Barnabas Poczos<sup>2</sup> Ruslan Ssalakhutdinov<sup>2</sup>  
Alexander Smola<sup>1,2</sup>

## Abstract

In this paper, we study the problem of designing objective functions for machine learning problems defined on finite *sets*. In contrast to traditional objective functions defined for machine learning problems operating on finite dimensional vectors, the new objective functions we propose are operating on finite sets and are invariant to permutations. Such problems are widespread, ranging from estimation of population statistics (Poczos et al., 2013), via anomaly detection in piezometer data of embankment dams (Jung et al., 2015), to cosmology (Ntampaka et al., 2016; Ravanbakhsh et al., 2016a). Our main theorem characterizes the permutation invariant objective functions and provides a family of functions to which any permutation invariant objective function must belong. This family of functions has a special structure which enables us to design a deep network architecture that can operate on sets and which can be deployed on a variety of scenarios including both unsupervised and supervised learning tasks. We demonstrate the applicability of our method on population statistic estimation, point cloud classification, set expansion, and image tagging.

## 1. Introduction

Classification and regression are among the most fundamental supervised learning problems. The most frequently used learning algorithms, however, can only deal with fixed, finite-dimensional representations, and researchers only recently started to investigate the case when the inputs or outputs are permutation invariant sets rather than finite dimensional vectors (Oliva et al., 2013; Szabo et al., 2016; Muandet et al., 2013; 2012). Supervised learning examples include tasks like estimation of population statistics (Poczos et al., 2013), where applications range from giga-scale cosmology (Ntampaka et al., 2016; Ravanbakhsh et al., 2016a) to nano-scale quantum chemistry (Faber et al., 2016).

Similarly, most unsupervised learning methods can only

---

<sup>1</sup>Amazon Web Services <sup>2</sup>Carnegie Mellon University, Pittsburgh PA. Correspondence to: Manzil Zaheer <manzil@cmu.edu>.

Work done while at Carnegie Mellon University.

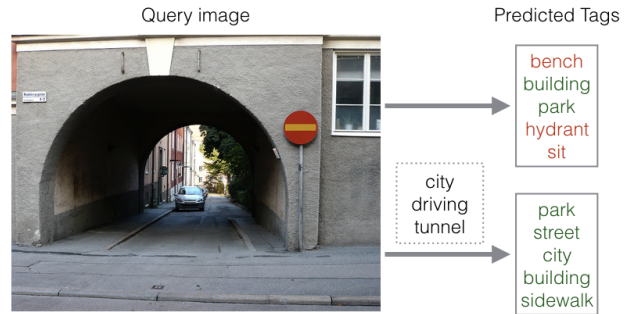


Figure 1. Illustration of Deepsets using image tagging task. Given a query image, predicted tags can be irrelevant (red) due to visual imperfections. For instance, the model confuses the stop sign to a fire hydrant. However, conditioned on a set of relevant tags, Deepsets recovers more appropriate tags (green).

operate on finite dimensional vectors, but there are many important cases when we want the learning algorithm to be invariant to permutation of the elements of the input.

One such unsupervised learning problem is the set expansion (audience expansion), where given a set of objects that are similar to each other (e.g. set of words {lion, tiger, leopard}) our goal is to find new objects from a large pool of candidates such that the selected new objects are similar to the query set (e.g. find words like jaguar or cheetah among all English words). This is a standard problem in similarity search and metric learning, and a typical application is to find new image tags given a small set of possible tags. Likewise, in field of computational advertisement, given a set of high-value customers, the goal would be to find similar people. This is an important problem in many scientific applications, e.g. given a small set of interesting celestial objects, astrophysicists might want to find similar ones in large sky surveys.

Recent progress in deep learning (LeCun et al., 2015) has witnessed applications to other structured settings, including graphs (Bruna et al., 2013; Duvenaud et al., 2015), groups (Gens & Domingos, 2014; Christopher, 2014; Cohen & Welling, 2016), sequences and hierarchies (Irsoy & Cardie, 2014; Socher et al., 2013). We, however, will only focus on cases when the inputs are sets, but each instance may have a structure of its own, such as graph, image, or another set.

**Main contributions.** In this paper, i) we propose a fundamental architecture to deal with sets as inputs and show that the properties of this architecture are both necessary

and sufficient (Sec. 2). ii) We extend this architecture to allow for conditioning on arbitrary objects, and iii) based on this architecture we develop a *deep network* that can operate on sets with possibly different sizes (Sec. 3). We show that a simple parameter-sharing scheme enables a general treatment of sets within supervised and semi-supervised settings. iv) We demonstrate the applicability of our framework algorithm through various problems (Sec. 4).

## 2. Permutation Invariant Objective Functions

### 2.1. Problem Definition.

First we formally define our problem and review some relevant background information. Our goal is to create a permutation invariant objective function  $S()$  and assign a score  $S(X)$  to a set  $X = \{x_1, \dots, x_m\}$ . For example, this score can indicate coherence of the set or can be an estimate of some population statistic among others. Under unsupervised setting, we are given  $N$  examples of  $X_1, \dots, X_N$  each representing one valid coherent set, i.e. the  $i$ -th input  $X_i = \{X_{i,1}, \dots, X_{i,m_i}\}$  consists of  $m_i$  elements. The task would be to assign high scores to valid sets and low scores to improbable sets. Such score can be used for set expansion tasks, such as image tagging or audience expansion in field of computational advertisement.

In the supervised learning setting, we would also have access to labels  $y_1, \dots, y_N$  and the task would be to classify/regress with variable number of predictors while being permutation invariant w.r.t predictors. Examples might include entropy estimation or a sum of a variable number of MNIST digits.

In the next section we begin with exploring properties of a function that operates on sets as input and relate these properties to existing work.

### 2.2. Structure

A function  $f$  transforms its domain  $\mathcal{X}$  into its range  $\mathcal{Y}$ . Usually, the input domain is a vector space  $\mathbb{R}^d$  and the output response range is either a discrete space, e.g.  $\{0, 1\}$  in case of classification, or a continuous space  $\mathbb{R}$  in case of regression.

Now, if the input is a set  $X = \{x_1, \dots, x_m\}$ , then we would like the response of the function not to depend on the ordering of the elements in the set. In other words,

**Property 1** *A function  $f$  acting on sets must be permutation invariant to the order of objects in the set, i.e.*

$$f(\{x_1, \dots, x_m\}) = f(\{x_{\sigma(1)}, \dots, x_{\sigma(m)}\}) \quad (1)$$

for any permutation  $\sigma$ .

The next theorem characterizes the structure of permutation invariant functions.

**Theorem 2 (Universality)** *A function  $S(X)$  operating on a set  $X$  can be a valid scoring function, i.e. it is permutation invariant to the elements in  $X$ , if and only if it can be decomposed in the form  $\rho(\sum_{x \in X} \phi(x))$ , for suitable transformations  $\phi$  and  $\rho$ .*

**Proof sketch.** Permutation invariance follows from the fact that sets have no particular order, hence any function on a set must not exploit any particular order either. The sufficiency follows by observing that the function  $\rho(\sum_{x \in X} \phi(x))$  satisfies the permutation invariance condition.

To prove necessity, i.e. that all functions can be represented in this manner, note that polynomials are universal approximators. Hence it suffices if we prove the result for polynomials. In this case the Chevalley-Shephard-Todd (CST) theorem (Bourbaki, 1990, chap. V, theorem 4), or more precisely, its special case, the Fundamental Theorem of Symmetric Functions states that symmetric polynomials are given by a polynomial of homogeneous symmetric monomials. The latter are given by the sum over monomial terms, which is all that we need since it implies that all symmetric polynomials can be written in the form required by the theorem. ■

### 2.3. Specialization to Neural Network Layer

Now we consider how can we apply Theorem 2 to a deep network layer. Our goal is to design neural network layers that are invariant to permutations of elements in the input  $\mathbf{x}$ . Consider the standard neural network layer

$$\mathbf{f}_\Theta(\mathbf{x}) \doteq \sigma(\Theta \mathbf{x}) \quad \Theta \in \mathbb{R}^{N \times N} \quad (2)$$

where  $\Theta$  is the weight vector and  $\sigma : \mathbb{R} \rightarrow \mathbb{R}$  is a nonlinearity such as sigmoid function. The following lemma states the necessary and sufficient conditions for permutation-equivariance in this type of function.

**Lemma 3** *The function  $\mathbf{f}_\Theta : \mathbb{R}^N \rightarrow \mathbb{R}^N$  as defined in (2) is permutation invariant if and only if all the off-diagonal elements of  $\Theta$  are tied together and all the diagonal elements are equal as well. That is,*

$$\Theta = \lambda \mathbf{I} + \gamma (\mathbf{1}\mathbf{1}^T) \quad \lambda, \gamma \in \mathbb{R} \quad \mathbf{1} = [1, \dots, 1]^T \in \mathbb{R}^N$$

where  $\mathbf{I} \in \mathbb{R}^{N \times N}$  is the identity matrix.

This function is simply a non-linearity applied to a weighted combination of i) its input  $\mathbf{I}\mathbf{x}$  and; ii) the sum of input values  $(\mathbf{1}\mathbf{1}^T)\mathbf{x}$ . Since summation does not depend on the permutation, the layer is permutation-equivariant. Therefore we can manipulate the operations and parameters in this layer, for example to get another **variation**

$$\mathbf{f}(\mathbf{x}) \doteq \sigma(\lambda \mathbf{I}\mathbf{x} + \gamma \max\text{pool}(\mathbf{x})\mathbf{1}) \quad (3)$$

where the maxpooling operation over elements of the set (similarly to summation) is commutative. In practice using this variation performs better in some applications. This may be due to the fact that for  $\lambda = \gamma$ , the input to the non-linearity is max-normalized.

## 2.4. Other Related Results and Special Cases

**de Finetti theorem:** A related concept is that of an exchangeable model in Bayesian statistics, It is backed by deFinetti's theorem which states that:

$$p(X|\alpha) = \int d\theta \left[ \prod_{i=1}^m p(x_i|\theta) \right] p(\theta|\alpha). \quad (4)$$

To see that this fits into our result, let us consider exponential families with conjugate priors for illustration purpose, where we have

$$p(x|\theta) = \exp(\langle \phi(x), \theta \rangle - g(\theta)) \quad \text{and} \quad (5)$$

$$p(\theta|\alpha, m_0) = \exp(\langle \theta, \alpha \rangle - m_0 g(\theta) - h(\alpha, m_0)). \quad (6)$$

Now if we marginalize out  $\theta$ , we get a form which looks exactly like the one in Theorem 2, i.e.

$$P(X|\alpha) = \exp\left(h\left(\alpha + \sum_{x \in X} \phi(x), m_0 + m\right) - h(\alpha, m_0)\right)$$

**Representer theorem and kernel machines:** Support distribution machines use the following prediction function (Muandet et al., 2012; Poczos et al., 2012):

$$f(p) = \sum_i \alpha_i y_i K(p_i, p) + b, \quad (7)$$

where  $p_i, p$  are distributions and  $\alpha_i, b \in \mathbb{R}$ . In practice the  $p_i, p$  distributions are never given to us explicitly, usually only i.i.d. sample sets are available from these distributions, and therefore we need to estimate kernel  $K(p, q)$  using these samples. A popular approach is to use  $\hat{K}(p, q) = \frac{1}{MN} \sum_{i,j} k(x_i, y_j)$ , where  $k$  is another kernel operating on the samples  $\{x_i\}_{i=1}^N \sim p$  and  $\{y_j\}_{j=1}^M \sim q$ . Now (7) can be seen fitting into above defined structure.

**Spectral methods:** A consequence of the polynomial decomposition is that spectral methods (Anandkumar et al., 2012) can be viewed as a special case of the mapping  $\rho \circ \phi(X)$ : in that case one can compute polynomials, usually only up to a relatively low degree (such as  $k = 3$ ), to perform inference about statistical properties of the distribution. The statistics are exchangeable in the data, hence they could be represented by the above map.

## 3. Deep Sets

### 3.1. Architecture

The structure of permutation invariant functions which we got in Theorem 2 hints to an alternative strategy for inferring

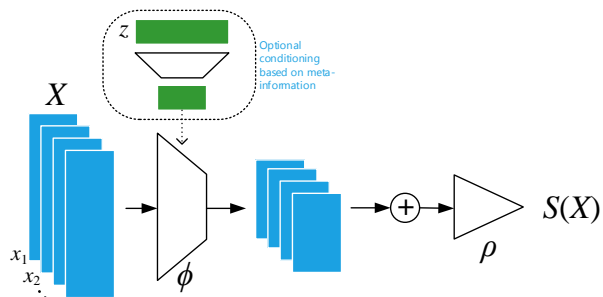


Figure 2. Architecture of deep sets

sets of objects — deep sets. Replacing  $\phi$  and  $\rho$  by universal approximators leaves matters unchanged, since, in particular,  $\phi$  and  $\rho$  can be used to approximate arbitrary polynomials. Then, it remains to learn these approximators. This yields in the following model:

- Each input  $x$  is transformed (possibly by several layers) into some representation  $\phi(x)$ .
- The representations are added up and their output is the processed using the  $\rho$  network very much in the same manner as in any deep network (e.g. fully connected layers, nonlinearities, etc.).
- Optionally: If we have additional meta-information  $z$ , then the above mentioned networks could be conditioned to obtain the conditioning mapping  $\phi(x|z)$ .

In other words, the key to deep sets is to add up all representations and then apply nonlinear transformations. The overall model structure is illustrated in Fig. 2.

This architecture has a number of desirable properties in terms of universality and correctness. We assume in the following that the networks we choose are, in principle, universal approximators. That is, we assume that they can represent any functional mapping. This is a well established property (see e.g. (Micchelli, 1986) for details in the case of radial basis function networks).

What remains is to state the derivatives with regard to this novel type of layer. Assume parametrizations  $w_\rho$  and  $w_\phi$  for  $\rho$  and  $\phi$  respectively. Then we have

$$\partial_{w_\phi} \rho \left( \sum_{x' \in X} \phi(x') \right) = \rho' \left( \sum_{x' \in X} \phi(x') \right) \sum_{x' \in X} \partial_{w_\phi} \phi(x')$$

This result reinforces the common knowledge of parameter tying in deep networks when ordering is irrelevant. Our result backs this practice with theory and strengthens it by proving that it is the only way to do it.

### 3.2. Application: Set Regression Scalar Response

Learning real valued functionals of distributions (e.g. entropy, mutual information) is of great importance in statistics and machine learning. For certain functionals, however, this is very difficult, especially if our only information about the density is based on a few i.i.d. samples. This is a regression task on sample sets with scalar response. Using the

DeepSets neural network defined above, we can estimate the unknown function  $f : \mathcal{X} \rightarrow \mathbb{R}$  directly in a supervised fashion, where  $\mathcal{X}$  is the space of set inputs.

### 3.3. Application: Set Expansion

In the set expansion task, we are given a set of objects that are similar to each other and our goal is to find new objects from a large pool of candidates such that the selected new objects are similar to the query set. To achieve this one needs to reason out the concept connecting the given set and then retrieve words based on their relevance to the inferred concept. It is an important task due to wide range of potential applications including personalized information retrieval, computational advertisement, tagging large amounts of unlabeled or weakly labeled datasets, *etc.*

If we go back to de Finetti’s theorem in Sec. 2.4, where we consider the marginal probability of a set of observations, the marginal probability allows for very simple metric for scoring additional elements to be added to  $X$ . In other words, this allows one to perform set expansion simply via the following score

$$s(x|X) = \log \frac{p(X \cup \{x\}|\alpha)}{p(X|\alpha)p(\{x\}|\alpha)} \quad (8)$$

Note that  $s(x|X)$  is the pointwise mutual information between  $x$  and  $X$ . Moreover, due to exchangeability, it follows that regardless of the order of elements we have

$$S(X) := \sum_{i=1}^m s(x_i|\{x_{i-1}, \dots, x_1\}) \quad (9)$$

$$= \log p(X|\alpha) - \sum_{i=1}^m \log p(\{x_i\}|\alpha) \quad (10)$$

In other words, we have a set function  $\log p(X|\alpha)$  with a modular term-dependent correction. When inferring sets, our goal is to find set completions  $\{x_{n+1}, \dots, x_m\}$  for an initial set of query terms  $\{x_1, \dots, x_n\}$ , such that the aggregate set is coherent. This is the key idea of the Bayesian Set algorithm (Ghahramani & Heller, 2005b).

Using DeepSets, we can solve this problem in more generality as we can drop the assumption of data belonging to certain exponential family. In the simplest case, we could learn the DeepSets network by trying to maximize the discriminative score  $s(x|X)$  such that the terms to be added obtain a large value.

While this improves discriminative performance, it does not necessarily take the relative similarity of objects into account. In particular, it does not guarantee large margin ranking performance such that the score  $s(x_{ij}|X_i \setminus \{x_{ij}\})$  is much larger than  $s(x|X_i \setminus \{x_{ij}\})$  for any  $x \notin X_i$ . Instead, we take recourse to large-margin classification with structured loss functions (Taskar et al., 2004) to obtain the relative loss objective

$$l(x, x'|X) := \max(0, s(x'|X) - s(x|X) + \Delta(x, x')) \quad (11)$$

In other words, we want to ensure that  $s(x|X) \geq s(x'|X) + \Delta(x, x')$  whenever  $x$  should be added and  $x'$  should not be added to  $X$ .

### 3.4. Conditioning

Often machine learning problems do not exist in isolation. For example, task like tag completion from a given set of tags is usually related to an object  $z$ , for example an image, that needs to be tagged. Such meta-data are usually abundant, e.g. author information in case of text, contextual data such as the user click history, or extra information collected with LiDAR point cloud.

Conditioning graphical models with such meta-data is often complicated, e.g. ensuring that the conditional representation  $\phi(x|z)$  is contained inside the correct marginal polytope is not always trivial. For instance, for the Beta-Binomial model we need to ensure that the counts are always nonnegative, regardless of  $z$ . Fortunately, DeepSets does not suffer from such complications and the fusion of multiple sources of data can be done in a relatively straightforward manner. Any of the existing methods in deep learning, including feature concatenation by averaging, or by max-pooling, can be employed as shown in Fig. 2. Incorporating these meta-data often leads to significantly improved performance as we will show in our experiments (Sec. 4.2.2).

## 4. Experiments

We now present an empirical study for our permutation invariant DeepSets model. First, we show experiments for supervised regression and classification setting in Sec. 4.1. Next, we consider semi-supervised tasks of set expansion (Sec. 4.2) and set anomaly detection (Sec. 4.3).

### 4.1. Set Input Scalar Response

#### 4.1.1. POPULATION STATISTIC ESTIMATION

In the first set experiment, we learn the entropy and mutual information of Gaussian distributions, without providing any information about Gaussianity to DeepSets. The Gaussian distributions are generated as follows:

- **Rotation:** We randomly chose a  $2 \times 2$  covariance matrix  $\Sigma$ , and then generated  $N$  sample sets from  $\mathcal{N}(0, R(\alpha)\Sigma R(\alpha)^T)$  of size  $M = [300 - 500]$  for  $N$  random values of  $\alpha \in [0, \pi]$ . Our goal was to learn the entropy of the marginal distribution of first dimension.
- **Correlation:** We randomly chose a  $d \times d$  covariance matrix  $\Sigma$  for  $d = 16$ , and then generated  $N$  sample sets from  $\mathcal{N}(0, [\Sigma, \alpha\Sigma; \alpha\Sigma, \Sigma])$  of size  $M = [300 - 500]$  for  $N$  random values of  $\alpha \in (-1, 1)$ . Goal was to learn the mutual information of among the first  $d$  and last  $d$  dimension.
- **Random:** We chose  $N$  random  $d \times d$  covariance matrix  $\Sigma$  for  $d = 32$ , and then using each generated a sample set from  $\mathcal{N}(0, \Sigma)$  of size  $M = [300 - 500]$ . Goal was to

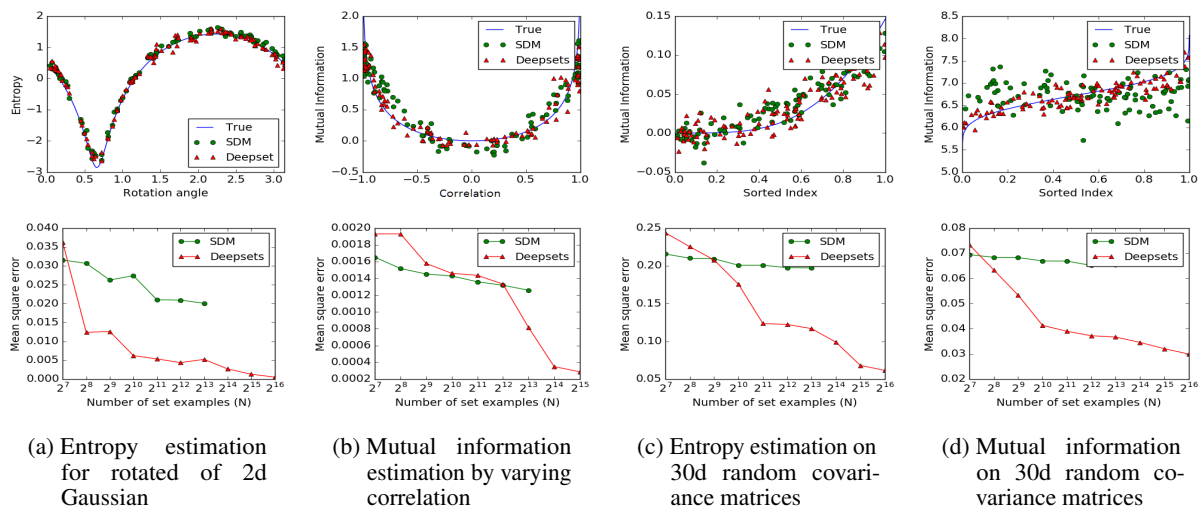


Figure 3. Set regression scalar response: Top set of figures, show prediction of DeepSets vs SDM for  $N = 2^{10}$  case. Bottom set of figures, depict the mean squared error behavior as number of sets is increased. SDM has lower error for small number of examples and DeepDets requires more data to reach similar accuracy. But for high dimensional problems deep sets easily *scales* to large number of examples and produces much *lower* estimation error.

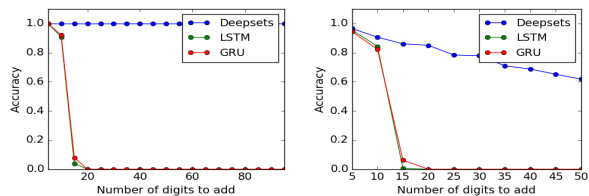


Figure 4. Accuracy of digit summation. On left is the case with text input and on right is the case with image based input. Training is done on tasks of length 10 at most, while at test time we use examples of length up to 100. We can see that DeepSets generalize much better.

learn the joint entropy and mutual information.

We learn this using an  $L_2$  loss with a DeepSet architecture having 3 fully connected layers with ReLU activation for both transformations  $\phi$  and  $\rho$ . We compare against Support Distribution Machines (SDM) using a RBF kernel (Poczos et al., 2012). The results are shown in Fig. 3. SDM has lower error for small number of examples and DeepDets requires more data to reach similar accuracy. But for high dimensional problems deep sets easily *scales* to large number of examples and produces much *lower* estimation error.

#### 4.1.2. SUM OF DIGITS

Next, we compare to what happens if our set data is treated as a sequence. We consider the task of finding sum of a given set of digits. We consider two variants of this experiment:

**Text** We randomly sample a subset of maximum  $N = 10$  digits from this dataset to build 100,000 sets of training images, where the set-label is the sum of digits in that set. We test against sums of  $N$  digits, for  $N$  starting from 5 all the way up to 100 over another 100,000 examples.

**Image** MNIST8m dataset (Loosli et al., 2007) contains 8 million instances of 28x28 grey-scale stamps of digits in

$\{0, \dots, 9\}$ . We randomly sample a subset of  $N$  images from this dataset to build 100,000 sets of training and 100,000 sets of test images, where the set-label is the sum of digits in that set (i.e., individual labels per image is unavailable). We test against sums of  $N$  digits, for  $N$  starting from 5 all the way up to 50.

We compare against recurrent neural networks – LSTM and GRU. All models are defined to have similar number of layers and parameters. The output of all models is a scalar, predicting the sum of  $N$  digits. Training is done on tasks of length 10 at most, while at test time we use examples of length upto 100. The accuracy, i.e. exact equality after rounding, is shown in Fig. 4. DeepSets generalize much better. Note for image case, the best classification error for single digit is around  $p = 0.01$  for MNIST8m, so in a collection of  $N$  of images at least one image will be misclassified is  $1 - (1 - p)^N$ , which is 40% for  $N = 50$ . This matches closely with observed value in Fig. 4(b).

#### 4.1.3. IMPROVED RED-SHIFT ESTIMATION USING CLUSTERING INFORMATION

An important regression problem in cosmology is to estimate the red-shift of galaxies, corresponding to their age as well as their distance from us (Binney & Merrifield, 1998) based on photometric observations. One way to estimate the red-shift from photometric observations is using a regression model (Connolly et al., 1995) on the galaxy clusters. The prediction for each galaxy does not change by permuting the members of the galaxy cluster. Therefore, we can treat each galaxy cluster as a “set” and use DeepSet to estimate the individual galaxy red-shifts.

For each galaxy, we have 17 photometric features from the

Model	Instance Size	Representation	Accuracy
3DShapeNets (Wu et al., 2015)	$30^3$	voxels (using convolutional deep belief net)	77%
DeepPano (Shi et al., 2015)	$64 \times 160$	panoramic image (2D CNN + angle-pooling)	77.64%
VoxNet (Maturana & Scherer, 2015)	$32^3$	voxels (voxels from point-cloud + 3D CNN)	83.10%
MVCNN (Su et al., 2015)	$164 \times 164 \times 12$	multi-view images (2D CNN + view-pooling)	90.1%
VRN Ensemble (Brock et al., 2016)	$32^3$	voxels (3D CNN, variational autoencoder)	95.54%
3D GAN (Wu et al., 2016)	$64^3$	voxels (3D CNN, generative adversarial training)	83.3%
DeepSsets	$5000 \times 3$	point-cloud	$90 \pm .3\%$

Table 2. Classification accuracy and the (size of) representation used by different methods on the ModelNet40 dataset.

redMaPPer galaxy cluster catalog (Roza & Rykoff, 2014) that contains photometric readings for 26,111 red galaxy clusters. Each galaxy-cluster in this catalog has between  $\sim 20 - 300$  galaxies – i.e.  $\mathbf{x} \in \mathbb{R}^{N(c) \times 17}$ , where  $N(c)$  is the cluster-size. The catalog also provides accurate spectroscopic red-shift estimates for a *subset* of these galaxies.

We randomly split the data into 90% training and 10% test clusters, and minimize the squared loss of the prediction for available spectroscopic red-shifts. As it is customary in cosmology literature, we report the average **scatter**  $\frac{|z_{\text{spec}} - z|}{1 + z_{\text{spec}}}$ , where  $z_{\text{spec}}$  is the accurate spectroscopic measurement and  $z$  is a photometric estimate in table 1.

Method	Average scatter
MLP	0.026
redMaPPer	0.025
DeepSets	0.023

Table 1. Red shift experiment. Lower scatter is better.

#### 4.1.4. POINT CLOUD CLASSIFICATION

A low-dimensional point-cloud is a set of low-dimensional vectors. This type of data is frequently encountered in various applications from robotics and vision to cosmology. In these applications, point-cloud data is often converted to voxel or mesh representation at a preprocessing step (e.g. Maturana & Scherer, 2015; Ravanbakhsh et al., 2016b; Lin et al., 2004). Since the output of many range sensors, such as LiDAR, is in the form of point-cloud, direct application of deep learning methods to point-cloud is highly desirable. Moreover, when working with point-clouds rather than voxelized 3D objects, it is easy to apply transformations such as rotation and translation as differentiable layers at low cost.

As point-cloud data is just a set of points, we can use DeepSets to classify point-cloud representation of a subset of ShapeNet objects (Chang et al., 2015), called ModelNet40 (Wu et al., 2015). This subset consists of 3D representation of 9,843 training and 2,468 test instances belonging to 40 classes of objects. We produce point-clouds with 100, 1000 and 5000 particles each ( $x, y, z$ -coordinates) from the mesh representation of objects using the point-cloud-library’s sampling routine (Rusu & Cousins, 2011). Each set is normalized by the initial layer of the deep network to have zero mean (along individual axes) and unit (global) variance.

Table 6 compares our method against the competition.<sup>1</sup> Note that we achieve our best accuracy using  $5000 \times 3$  dimensional representation of each object, which is much smaller than most other methods. All other techniques use either voxelization or multiple view of the 3D object for classification.

## 4.2. Set Expansion

### 4.2.1. TEXT CONCEPT SET RETRIEVAL

We consider the task of text concept set retrieval, where the objective is to retrieve words belonging to a ‘concept’ or ‘cluster’, given few words from that particular concept. For example, given the set of words  $\{tiger, lion, cheetah\}$ , we would need to retrieve other related words like *jaguar, puma, etc*, which belong to the same concept of big cats. This task of concept set retrieval can be seen as a set completion task conditioned on the latent semantic concept, and therefore our DeepSets form a desirable approach.

**Dataset** We construct a large dataset containing sets of  $N_T = 50$  related words by extracting topics from latent Dirichlet allocation (Pritchard et al., 2000; Blei et al., 2003), taken out-of-the-box<sup>2</sup>. To compare across scales, we consider three values of  $k = \{1k, 3k, 5k\}$  giving us three datasets LDA-1k, LDA-3k, and LDA-5k, with corresponding vocabulary sizes of 17k, 38k, and 61k.

**Methods** We learn this using a margin loss with a DeepSet architecture having 3 fully connected layers with ReLU activation for both transformations  $\phi$  and  $\rho$ . Details of the architecture and training are in Appendix B. We compare to several baselines: (a) **Random** picks a word from the vocabulary uniformly at random. (b) **Bayes Set** (Ghahramani & Heller, 2005b), and (c) **w2v-Near** that computes the nearest neighbors in the word2vec (Mikolov et al., 2013) space. Note that both Bayes Set and w2v NN are strong baselines. The former runs Bayesian inference using Beta-Binomial conjugate pair, while the latter uses the powerful 300 dimensional word2vec trained on the billion word Google-

<sup>1</sup>The error-bar on our results is due to variations depending on the choice of particles during test time and it is estimated over three trials.

<sup>2</sup>[github.com/dmlc/experimental-lda](https://github.com/dmlc/experimental-lda)

## Deep Sets

Method	LDA-1k (Vocab = 17k)					LDA-3k (Vocab = 38k)					LDA-5k (Vocab = 61k)				
	Recall (%)			MRR	Med.	Recall (%)			MRR	Med.	Recall (%)			MRR	Med.
	@10	@100	@1k			@10	@100	@1k			@10	@100	@1k		
Random	0.06	0.6	5.9	0.001	8520	0.02	0.2	2.6	0.000	28635	0.01	0.2	1.6	0.000	30600
Bayes Set	1.69	11.9	37.2	0.007	2848	2.01	14.5	36.5	0.008	3234	1.75	12.5	34.5	0.007	3590
w2v Near	<b>6.00</b>	<b>28.1</b>	<b>54.7</b>	0.021	<b>641</b>	4.80	21.2	43.2	0.016	2054	4.03	16.7	35.2	0.013	6900
NN-max	4.78	22.5	53.1	0.023	779	5.30	24.9	54.8	0.025	672	4.72	21.4	47.0	0.022	1320
NN-sum-con	4.58	19.8	48.5	0.021	1110	5.81	27.2	60.0	<b>0.027</b>	453	4.87	23.5	53.9	0.022	731
NN-max-con	3.36	16.9	46.6	0.018	1250	5.61	25.7	57.5	0.026	570	4.72	22.0	51.8	0.022	877
DeepSets	5.53	24.2	54.3	<b>0.025</b>	696	<b>6.04</b>	<b>28.5</b>	<b>60.7</b>	<b>0.027</b>	<b>426</b>	<b>5.54</b>	<b>26.1</b>	<b>55.5</b>	<b>0.026</b>	<b>616</b>

Table 3. Results on Text Concept Set Retrieval on LDA-1k, LDA-3k, and LDA-5k. Our Deepsets model outperforms other methods on LDA-3k and LDA-5k. However, all neural network based methods have inferior performance to w2v-Near baseline on LDA-1k, possibly due to small data size. Higher the better for recall@k and mean reciprocal rank (MRR). Lower the better for median rank (Med.)

News corpus<sup>3</sup>. (d) **NN-max** uses a similar architecture as our DeepSet model with an important difference. It uses max pooling to compute the set feature, as opposed to DeepSets which uses sum pooling. (e) **NN-max-con** uses max pooling on set elements but concatenates this pooled representation with that of query for a final set feature. (f) **NN-sum-con** is similar to NN-max-con but uses sum pooling followed by concatenation with query representation.

**Evaluation** To quantitatively evaluate, we consider the standard retrieval metrics – recall@K, median rank and mean reciprocal rank. To elaborate, recall@K measures the number of true labels that were recovered in the top K retrieved words. We use three values of  $K = \{10, 100, 1k\}$ . The other two metrics, as the names suggest, are the median and mean of reciprocals of the true label ranks, respectively. Each dataset is split into TRAIN (80%), VAL (10%) and TEST (10%). We learn models using TRAIN and evaluate on TEST, while VAL is used for hyperparameter selection and early stopping.

**Results and Observations** Tab. 3 contains the results for the text concept set retrieval on LDA-1k, LDA-3k, and LDA-5k datasets. We summarize our findings below: (a) Our DeepSets model outperforms all other approaches on LDA-3k and LDA-5k by any metric, highlighting the significance of permutation invariance property. For instance, DeepSets is better than the w2v-Near baseline by 1.5% in Recall@10 on LDA-5k. (b) On LDA-1k, neural network based models do not perform well when compared to w2v-Near. We hypothesize that this is due to small size of the dataset insufficient to train a high capacity neural network, while w2v-Near has been trained on a billion word corpus. Nevertheless, our approach comes the closest to w2v-Near amongst other approaches, and is only 0.5% lower by Recall@10.

### 4.2.2. IMAGE TAGGING

We next experiment with image tagging, where the task is to retrieve all relevant tags corresponding to an image. Images usually have only a subset of relevant tags, therefore predicting other tags can help enrich information that can further be leveraged in a downstream supervised task. In

<sup>3</sup>[code.google.com/archive/p/word2vec/](http://code.google.com/archive/p/word2vec/)

Method	ESP game				IAPRTC-12.5			
	P	R	F1	N+	P	R	F1	N+
Least Sq.	35	19	25	215	40	19	26	198
MBRM	18	19	18	209	24	23	23	223
JEC	24	19	21	222	29	19	23	211
FastTag	46	22	30	<b>247</b>	<b>47</b>	26	34	<b>280</b>
Least Sq.(D)	<b>44</b>	32	<b>37</b>	232	46	30	36	218
FastTag(D)	<b>44</b>	32	<b>37</b>	229	46	<b>33</b>	<b>38</b>	254
DeepSets	39	<b>34</b>	36	246	42	31	36	247

Table 4. Results of image tagging on ESPgame and IAPRTC-12.5 datasets. Performance of our Deepsets approach is roughly similar to the best competing approaches, except for precision. Refer text for more details. Higher the better for all metrics – precision (P), recall (R), f1 score (F1), and number of non-zero recall tags (N+).

Method	Recall			MRR	Med.
	@10	@100	@1k		
w2v NN (blind)	5.6	20.0	54.2	0.021	823
DeepSets (blind)	9.0	39.2	71.3	0.044	310
DeepSets	<b>31.4</b>	<b>73.4</b>	<b>95.3</b>	<b>0.131</b>	<b>28</b>

Table 5. Results on COCO-Tag dataset. Clearly, Deepsets outperforms other baselines significantly. Higher the better for recall@K and mean reciprocal rank (MRR). Lower the better for median rank (Med). All models use a set size of 5 to predict tags.

our setup, we learn to predict tags by conditioning DeepSets on the image. Specifically, we train by learning to predict a partial set of tags from the image and remaining tags. At test time, we the test image is used to predict relevant tags.

**Datasets** We report results on the following three datasets - ESPGame, IAPRTC-12.5 and our in-house dataset, COCO-Tag. Due to lack of space, we refer the reader to Appendix C, for more details about datasets.

**Methods** The setup for DeepSets to tag images is similar to that described in Sec. 4.2.1. The only difference being the conditioning on the image features, which is concatenated with the set feature obtained from pooling individual element representations.

**Baselines** We perform comparisons against several baselines, previously reported in (Chen et al., 2013). Specifically, we have Least Sq., a ridge regression model, MBRM (Feng



Figure 5. Each row shows a set, constructed from CelebA dataset, such that all set members except for an outlier, share at least two attributes (on the right). The outlier is identified with a red frame. The model is trained by observing examples of sets and their anomalous members, **without access to the attributes**. The probability assigned to each member by the outlier detection network is visualized using a red bar at the bottom of each image. The probabilities in each row sum to one.

et al., 2004), JEC (Makadia et al., 2008) and FastTag (Chen et al., 2013). Note that these methods do not use deep features for images, which could lead to an unfair comparison. As there is no publicly available code for MBRM and JEC, we cannot get performances of these models with Resnet extracted features. However, we report results with deep features for FastTag and Least Sq., using code made available by the authors<sup>4</sup>.

**Evaluation** For ESPgame and IAPRTC-12.5, we follow the evaluation metrics as in (Guillaumin et al., 2009) – precision (P), recall (R), F1 score (F1) and number of tags with non-zero recall (N+). Note that these metrics are evaluate for each tag and the mean is reported. We refer to (Guillaumin et al., 2009) for further details. For COCO-Tag, however, we use recall@K for three values of  $K = \{10, 100, 1000\}$ , along with median rank and mean reciprocal rank (see evaluation in Sec. 4.2.1 for metric details).

**Results and Observations** Tab. 4 contains the results of image tagging on ESPgame and IAPRTC-12.5, and Tab. 5 on COCO-Tag. Here are the key observations from Tab. 4: (a) The performance of our DeepSets model is comparable to the best approaches on all metrics but precision. (b) Our recall beats the best approach by 2% in ESPgame. On further investigation, we found that the DeepSets model retrieves more relevant tags, which are not present in list of ground truth tags due to a limited 5 tag annotation. Thus, this takes a toll on precision while gaining on recall, yet yielding improvement in F1. On the larger and richer COCO-Tag, we see that the DeepSets approach outperforms other methods comprehensively, as expected. We show qualitative examples in Appendix C.

### 4.3. Set Anomaly Detection

The objective here is to find the anomalous face in each set, simply by observing examples and without any access to the attribute values. CelebA dataset (Liu et al., 2015) contains 202,599 face images, each annotated with 40 boolean attributes. We use  $64 \times 64$  stamps and using these attributes

we build 18,000 sets, each containing  $N = 16$  images (on the training set) as follows: after randomly selecting two attributes, we draw 15 images where those attributes are present and a single image where both attributes are absent. Using a similar procedure we build sets on the test images. No individual person’s face appears in both train and test sets.

Our deep neural network consists of 9 2D-convolution and max-pooling layers followed by 3 permutation-equivariant layers and finally a softmax layer that assigns a probability value to each set member (Note that one could identify arbitrary number of outliers using a sigmoid activation at the output.) Our trained model successfully finds the anomalous face in **75% of test sets**. Visually inspecting these instances suggests that the task is non-trivial even for humans; see Fig. 5.

As a *baseline*, we repeat the same experiment by using a set-pooling layer after convolution layers, and replacing the permutation-equivariant layers with fully connected layers, with the same number of hidden units/output-channels, where the final layer is a 16-way softmax. The resulting network shares the convolution filters for all instances within all sets, however the input to the softmax is not equivariant to the permutation of input images. Permutation equivariance seems to be crucial here as the baseline model achieves a training and **test accuracy of  $\sim 6.3\%$** ; the same as random selection.

Detailed experimental setup and results for each of the experiment is provided in the Appendix.

## 5. Summary

In this paper we developed DeepSets model based on the powerful permutation invariance property along with theory to support its performance. We demonstrated the generalization ability of DeepSets across several domains by extensive experiments, and showed both qualitative and quantitative results.

<sup>4</sup><http://www.cse.wustl.edu/~mchen/>



## References

- Anandkumar, A., Ge, R., Hsu, D., Kakade, S. M., and Tlupova, M. Tensor decompositions for learning latent variable models. *arXiv preprint arXiv:1210.7559*, 2012.
- Binney, James and Merrifield, Michael. *Galactic astronomy*. Princeton University Press, 1998.
- Blei, David M., Ng, Andrew Y., Jordan, Michael I., and Lafferty, John. Latent dirichlet allocation. *Journal of Machine Learning Research*, 3:2003, 2003.
- Bourbaki, Nicolas. *Éléments de mathématiques: théorie des ensembles, chapitres 1 à 4*, volume 1. Masson, 1990.
- Brock, Andrew, Lim, Theodore, Ritchie, JM, and Weston, Nick. Generative and discriminative voxel modeling with convolutional neural networks. *arXiv preprint arXiv:1608.04236*, 2016.
- Bruna, Joan, Zaremba, Wojciech, Szlam, Arthur, and LeCun, Yann. Spectral networks and locally connected networks on graphs. *arXiv preprint arXiv:1312.6203*, 2013.
- Chang, Angel X, Funkhouser, Thomas, Guibas, Leonidas, Hanrahan, Pat, Huang, Qixing, Li, Zimo, Savarese, Silvio, Savva, Manolis, Song, Shuran, Su, Hao, et al. Shapenet: An information-rich 3d model repository. *arXiv preprint arXiv:1512.03012*, 2015.
- Chen, Minmin, Zheng, Alice, and Weinberger, Kilian. Fast image tagging. In *Proceedings of The 30th International Conference on Machine Learning*, pp. 1274–1282, 2013.
- Christopher, Olah. Groups and group convolutions. <http://colah.github.io/posts/2014-12-Groups-Convolution/>, 2014.
- Clevert, Djork-Arné, Unterthiner, Thomas, and Hochreiter, Sepp. Fast and accurate deep network learning by exponential linear units (elus). *arXiv preprint arXiv:1511.07289*, 2015.
- Cohen, Taco S and Welling, Max. Group equivariant convolutional networks. *arXiv preprint arXiv:1602.07576*, 2016.
- Connolly, AJ, Csabai, I, Szalay, AS, Koo, DC, Kron, RG, and Munn, JA. Slicing through multicolor space: Galaxy redshifts from broadband photometry. *arXiv preprint astro-ph/9508100*, 1995.
- Duvenaud, David K, Maclaurin, Dougal, Iparraguirre, Jorge, Bombarell, Rafael, Hirzel, Timothy, Aspuru-Guzik, Alán, and Adams, Ryan P. Convolutional networks on graphs for learning molecular fingerprints. In *Advances in Neural Information Processing Systems*, pp. 2224–2232, 2015.
- Faber, Felix A., Lindmaa, Alexander, von Lilienfeld, O. Anatole, and Armiesto, Rickard. Machine learning energies of 2 million elpasolite ( $abC_2D_6$ ) crystals. *Phys. Rev. Lett.*, 117:135502, Sep 2016. doi: 10.1103/PhysRevLett.117.135502. URL <http://link.aps.org/doi/10.1103/PhysRevLett.117.135502>.
- Feng, S. L., Manmatha, R., and Lavrenko, V. Multiple bernoulli relevance models for image and video annotation. In *Proceedings of the 2004 IEEE Computer Society Conference on Computer Vision and Pattern Recognition, CVPR'04*, pp. 1002–1009, Washington, DC, USA, 2004. IEEE Computer Society. URL <http://dl.acm.org/citation.cfm?id=1896300.1896446>.
- Gens, Robert and Domingos, Pedro M. Deep symmetry networks. In *Advances in neural information processing systems*, pp. 2537–2545, 2014.
- Ghahramani, Z. and Heller, K. Bayesian sets. In *Neural Information Processing Systems*, 2005a.
- Ghahramani, Zoubin and Heller, Katherine A. Bayesian sets. In *NIPS*, volume 2, pp. 22–23, 2005b.
- Grubinger, Michael. Analysis and evaluation of visual information systems performance, 2007. URL <http://eprints.vu.edu.au/1435>. Thesis (Ph. D.)–Victoria University (Melbourne, Vic.), 2007.
- Guillaumin, Matthieu, Mensink, Thomas, Verbeek, Jakob, and Schmid, Cordelia. Tagprop: Discriminative metric learning in nearest neighbor models for image auto-annotation. In *Computer Vision, 2009 IEEE 12th International Conference on*, pp. 309–316. IEEE, 2009.
- Irsoy, Ozan and Cardie, Claire. Deep recursive neural networks for compositionality in language. In *Advances in Neural Information Processing Systems*, pp. 2096–2104, 2014.
- Jung, I., Berges, M., Garrett, J., and Poczos, B. Exploration and evaluation of ar, mpca and kl anomaly detection techniques to embankment dam piezometer data. *Advanced Engineering Informatics*, 2015.
- Kingma, Diederik and Ba, Jimmy. Adam: A method for stochastic optimization. *arXiv preprint arXiv:1412.6980*, 2014.
- LeCun, Yann, Bengio, Yoshua, and Hinton, Geoffrey. Deep learning. *Nature*, 521(7553):436–444, 2015.
- Lin, Hong-Wei, Tai, Chiew-Lan, and Wang, Guo-Jin. A mesh reconstruction algorithm driven by an intrinsic property of a point cloud. *Computer-Aided Design*, 36(1):1–9, 2004.
- Lin, Tsung-Yi, Maire, Michael, Belongie, Serge, Hays, James, Perona, Pietro, Ramanan, Deva, Dollár, Piotr, and Zitnick, C Lawrence. Microsoft coco: Common objects in context. In *European Conference on Computer Vision*, pp. 740–755. Springer, 2014.
- Liu, Ziwei, Luo, Ping, Wang, Xiaogang, and Tang, Xiaoou. Deep learning face attributes in the wild. In *Proceedings of International Conference on Computer Vision (ICCV)*, 2015.
- Loosli, Gaëlle, Canu, Stéphane, and Bottou, Léon. Training invariant support vector machines using selective sampling. In Bottou, Léon, Chapelle, Olivier, DeCoste, Dennis, and Weston, Jason (eds.), *Large Scale Kernel Machines*, pp. 301–320. MIT Press, Cambridge, MA., 2007.
- Makadia, Ameesh, Pavlovic, Vladimir, and Kumar, Sanjiv. A new baseline for image annotation. In *Proceedings of the 10th European Conference on Computer Vision: Part III, ECCV '08*, pp. 316–329, Berlin, Heidelberg, 2008. Springer-Verlag. ISBN 978-3-540-88689-1. doi: 10.1007/978-3-540-88690-7\_24. URL [http://dx.doi.org/10.1007/978-3-540-88690-7\\_24](http://dx.doi.org/10.1007/978-3-540-88690-7_24).

- Maturana, Daniel and Scherer, Sebastian. Voxnet: A 3d convolutional neural network for real-time object recognition. In *Intelligent Robots and Systems (IROS), 2015 IEEE/RSJ International Conference on*, pp. 922–928. IEEE, 2015.
- Micchelli, C. A. Interpolation of scattered data: distance matrices and conditionally positive definite functions. *Constructive Approximation*, 2:11–22, 1986.
- Mikolov, Tomas, Sutskever, Ilya, Chen, Kai, Corrado, Greg S, and Dean, Jeff. Distributed representations of words and phrases and their compositionality. In *Advances in neural information processing systems*, pp. 3111–3119, 2013.
- Muandet, K., Fukumizu, K., Dinuzzo, F., and Schoelkopf, B. Learning from distributions via support measure machines. In *In Proceeding of the 26th Annual Conference on Neural Information Processing Systems (NIPS 2012)*, 2012.
- Muandet, K., Balduzzi, D., and Schoelkopf, B. Domain generalization via invariant feature representation. In *In Proceeding of the 30th International Conference on Machine Learning (ICML 2013)*, 2013.
- Ntampaka, M., Trac, H., Sutherland, D., Fromenteau, S., Póczos, B., and Schneider, J. Dynamical mass measurements of contaminated galaxy clusters using machine learning. *The Astrophysical Journal*, 2016. URL <http://arxiv.org/abs/1509.05409>.
- Oliva, J., Póczos, B., and Schneider, J. Distribution to distribution regression. In *International Conference on Machine Learning (ICML)*, 2013.
- Póczos, B., Xiong, L., Sutherland, D., and Schneider, J. Support distribution machines, 2012. URL <http://arxiv.org/abs/1202.0302>.
- Póczos, B., Rinaldo, A., Singh, A., and Wasserman, L. Distribution-free distribution regression. In *International Conference on AI and Statistics (AISTATS), JMLR Workshop and Conference Proceedings*, 2013.
- Pritchard, Jonathan K., Stephens, Matthew, and Donnelly, Peter. Inference of population structure using multilocus genotype data. *Genetics*, 155(2):945–959, 2000. ISSN 0016-6731. URL <http://www.genetics.org/content/155/2/945>.
- Ravanbakhsh, M., Oliva, J., Fromenteau, S., Price, L., Ho, S., Schneider, J., and Póczos, B. Estimating cosmological parameters from the dark matter distribution. In *International Conference on Machine Learning (ICML)*, 2016a.
- Ravanbakhsh, Siamak, Oliva, Junier, Fromenteau, Sebastien, Price, Layne C, Ho, Shirley, Schneider, Jeff, and Póczos, Barnabás. Estimating cosmological parameters from the dark matter distribution. In *Proceedings of The 33rd International Conference on Machine Learning*, 2016b.
- Rozo, Eduardo and Rykoff, Eli S. redmapper ii: X-ray and sz performance benchmarks for the sdss catalog. *The Astrophysical Journal*, 783(2):80, 2014.
- Rusu, Radu Bogdan and Cousins, Steve. 3D is here: Point Cloud Library (PCL). In *IEEE International Conference on Robotics and Automation (ICRA)*, Shanghai, China, May 9-13 2011.
- Shi, Baoguang, Bai, Song, Zhou, Zhichao, and Bai, Xiang. Deeppano: Deep panoramic representation for 3-d shape recognition. *IEEE Signal Processing Letters*, 22(12): 2339–2343, 2015.
- Socher, Richard, Perelygin, Alex, Wu, Jean Y, Chuang, Jason, Manning, Christopher D, Ng, Andrew Y, and Potts, Christopher. Recursive deep models for semantic compositionality over a sentiment treebank. In *Proceedings of the conference on empirical methods in natural language processing (EMNLP)*, volume 1631, pp. 1642. Citeseer, 2013.
- Su, Hang, Maji, Subhransu, Kalogerakis, Evangelos, and Learned-Miller, Erik. Multi-view convolutional neural networks for 3d shape recognition. In *Proceedings of the IEEE International Conference on Computer Vision*, pp. 945–953, 2015.
- Szabo, Z., Sriperumbudur, B., Póczos, B., and Gretton, A. Learning theory for distribution regression. *Journal of Machine Learning Research*, 2016.
- Taskar, B., Guestrin, C., and Koller, D. Max-margin Markov networks. In Thrun, S., Saul, L., and Schölkopf, B. (eds.), *Advances in Neural Information Processing Systems 16*, pp. 25–32, Cambridge, MA, 2004. MIT Press.
- Von Ahn, Luis and Dabbish, Laura. Labeling images with a computer game. In *Proceedings of the SIGCHI conference on Human factors in computing systems*, pp. 319–326. ACM, 2004.
- Wu, Jiajun, Zhang, Chengkai, Xue, Tianfan, Freeman, William T, and Tenenbaum, Joshua B. Learning a probabilistic latent space of object shapes via 3d generative-adversarial modeling. *arXiv preprint arXiv:1610.07584*, 2016.
- Wu, Zhirong, Song, Shuran, Khosla, Aditya, Yu, Fisher, Zhang, Linguang, Tang, Xiaoou, and Xiao, Jianxiong. 3d shapenets: A deep representation for volumetric shapes. In *Proceedings of the IEEE Conference on Computer Vision and Pattern Recognition*, pp. 1912–1920, 2015.

## A. Bayes Set

Bayesian sets consider the problem of estimating the likelihood of subsets  $X$  of a ground set  $\mathcal{X}$ . In general this is achieved by an exchangeable model motivated by deFinetti's theorem concerning exchangeable distributions via

$$p(X|\alpha) = \int d\theta \left[ \prod_{i=1}^m p(x_i|\theta) \right] p(\theta|\alpha). \quad (12)$$

This allows one to perform set expansion, simply via the score

$$s(x|X) = \log \frac{p(X \cup \{x\}|\alpha)}{p(X|\alpha)p(\{x\}|\alpha)} \quad (13)$$

Note that  $s(x|X)$  is the pointwise mutual information between  $x$  and  $X$ . Moreover, due to exchangeability, it follows that regardless of the order of elements we have

$$S(X) := \sum_{i=1}^m s(x_i | \{x_{i-1}, \dots, x_1\}) = \log p(X|\alpha) - \sum_{i=1}^m \log p(\{x_i\}|\alpha) \quad (14)$$

In other words, we have a set function  $\log p(X|\alpha)$  with a modular term-dependent correction. When inferring sets it is our goal to find set completions  $\{x_{n+1}, \dots, x_m\}$  for an initial set of query terms  $\{x_1, \dots, x_n\}$  such that the aggregate set is well coherent. This is the key idea of the Bayesian Set algorithm.

### A.1. Exponential Family

In exponential families, the above approach assumes a particularly nice form whenever we have conjugate priors. Here we have

$$p(x|\theta) = \exp(\langle \phi(x), \theta \rangle - g(\theta)) \text{ and } p(\theta|\alpha, m_0) = \exp(\langle \theta, \alpha \rangle - m_0 g(\theta) - h(\alpha, m_0)). \quad (15)$$

The mapping  $\phi : x \rightarrow \mathcal{F}$  is usually referred as sufficient statistic of  $x$  which maps  $x$  into a feature space  $\mathcal{F}$ . Moreover,  $g(\theta)$  is the log-partition (or cumulant-generating) function. Finally,  $p(\theta|\alpha)$  denotes the conjugate distribution which is in itself a member of the exponential family. It has the normalization  $h(\alpha) = \int d\theta \exp(\langle \theta, \alpha \rangle - g(\theta))$ . The advantage of this is that  $s(x|X)$  and  $S(X)$  can be computed in closed form (Ghahramani & Heller, 2005a) via

$$s(X) = h(\alpha + \phi(X), m_0 + m) + (m - 1)h(\alpha, m_0) - \sum_{i=1}^m h(\alpha + \phi(x_i), m + 1) \quad (16)$$

$$s(x|X) = h(\alpha + \phi(\{x\} \cup X), m_0 + m + 1) + h(\alpha, m_0) - h(\alpha + \phi(X), m_0 + m) - h(\alpha + \phi(x), m + 1) \quad (17)$$

For convenience we defined the sufficient statistic of a set to be the sum over its constituents, i.e.  $\phi(X) = \sum_i \phi(x_i)$ . It allows for very simple computation and maximization over additional elements to be added to  $X$ , since  $\phi(X)$  can be precomputed.

### A.2. Beta-Binomial Model

The model is particularly simple when dealing with the Binomial distribution and its conjugate Beta prior, since the ratio of Gamma functions allows for simple expressions. In particular, we have

$$h(\beta) = \log \Gamma(\beta^+) + \log \Gamma(\beta^-) - \Gamma(\beta). \quad (18)$$

With some slight abuse of notation we let  $\alpha = (\beta^+, \beta^-)$  and  $m_0 = \beta^+ + \beta^-$ . Setting  $\phi(1) = (1, 0)$  and  $\phi(0) = (0, 1)$  allows us to obtain  $\phi(X) = (m^+, m^-)$ , i.e.  $\phi(X)$  contains the counts of occurrences of  $x_i = 1$  and  $x_i = 0$  respectively. This leads to the following score functions

$$s(X) = \log \Gamma(\beta^+ + m^+) + \log \Gamma(\beta^- + m^-) - \log \Gamma(\beta + m) \quad (19)$$

$$s(x|X) = \begin{cases} \log \frac{\beta^+ + m^+}{\beta + m} - \log \frac{\beta^+}{\beta} & \text{if } x = 1 \\ \log \frac{\beta^- + m^-}{\beta + m} - \log \frac{\beta^-}{\beta} & \text{otherwise} \end{cases} \quad (20)$$

This is the model used by (Ghahramani & Heller, 2005a) when estimating Bayesian Sets for objects. In particular, they assume that for any given object  $x$  the vector  $\phi(x) \in \{0; 1\}^d$  is a  $d$ -dimensional binary vector, where each coordinate is drawn independently from some Beta-Binomial model. The advantage of the approach is that it can be computed very efficiently while only maintaining minimal statistics of  $X$ .

In a nutshell, the *algorithmic* operations performed in the Beta-Binomial model are as follows:

$$s(x|X) = 1^\top \left[ \sigma \left( \sum_{i=1}^m \phi(x_i) + \phi(x) + \beta \right) - \sigma(\phi(x) + \beta) \right] \quad (21)$$

In other words, we sum over statistics of the candidates  $x_i$ , add a bias term  $\beta$ , perform a *coordinate-wise* nonlinear transform over the aggregate statistic (in our case a logarithm), and finally we aggregate over the so-obtained scores, weighing each contribution equally.  $s(X)$  is expressed analogously.

### A.3. Gauss Inverse Wishart Model

Before abstracting away the probabilistic properties of the model, it is worth paying some attention to the case where we assume that  $x_i \sim \mathcal{N}(\mu, \Sigma)$  and  $(\mu, \Sigma) \sim \text{NIW}(\mu_0, \lambda, \Psi, \nu)$ , for a suitable set of conjugate parameters. While the details are (arguably) tedious, the overall structure of the model is instructive.

First note that the sufficient statistic of the data  $x \in \mathbb{R}^d$  is now given by  $\phi(x) = (x, xx^\top)$ . Secondly, note that the conjugate log-partition function  $h$  amounts to computing *determinants* of terms involving  $\sum_i x_i x_i^\top$  and moreover, nonlinear combinations of the latter with  $\sum_i x_i$ .

The *algorithmic* operations performed in the Gauss Inverse Wishart model are as follows:

$$s(x|X) = \sigma \left( \sum_{i=1}^m \phi(x_i) + \phi(x) + \beta \right) - \sigma(\phi(x) + \beta) \quad (22)$$

Here  $\sigma$  is a nontrivial convex function acting on a (matrix, vector) pair and  $\phi(x)$  is no longer a trivial map but performs a nonlinear dimension altering transformation on  $x$ . We will use this general template to fashion the Deep Sets algorithm.

## B. Text Concept Set Retrieval

We consider the task of text concept set retrieval, where the objective is to retrieve words belonging to a ‘concept’ or ‘cluster’, given few words from that particular concept. For example, given the set of words  $\{tiger, lion, cheetah\}$ , we would need to retrieve other related words like *jaguar, puma, etc.*, which belong to the same concept of big cats. The model implicitly needs to reason out the concept connecting the given set and then retrieve words based on their relevance to the inferred concept. Concept set retrieval is an important due to wide range of potential applications including personalized information retrieval, tagging large amounts of unlabeled or weakly labeled datasets, *etc.* This task of concept set retrieval can be seen as a set completion task conditioned on the latent semantic concept, and therefore our Deepsets form a desirable approach.

**Dataset** To construct a large dataset containing sets of related words, we make use of Wikipedia text due to its huge vocabulary and concept coverage. First, we run topic modeling on publicly available wikipedia text with  $K$  number of topics. Specifically, we use the famous latent Dirichlet allocation (Pritchard et al., 2000; Blei et al., 2003), taken out-of-the-box<sup>5</sup>. Next, we choose top  $N_T = 50$  words for each latent topic as a set giving a total of  $K$  sets of size  $N_T$ . To compare across scales, we consider three values of  $k = \{1k, 3k, 5k\}$  giving us three datasets LDA-1k, LDA-3k, and LDA-5k, with corresponding vocabulary sizes of  $17k, 38k, \text{ and } 61k$ . Few of the topics from LDA-1k are visualized in Tab. 6.

**Methods** Our Deepsets model uses a feedforward neural network (NN) to represent a query and each element of a set, *i.e.*,  $\phi(x)$  for an element  $x$  is encoded as a NN. We then construct a set representation or feature, by sum pooling all the individual representations of its elements, along with that of the query. Note that this sum pooling achieves permutation invariance, a crucial property of our Deepsets (Theorem 2). Next, use input this set feature into another NN to assign a single score to the set, shown as  $\rho(\cdot)$ . In summary, our Deepsets consists of two neural networks – (a) to extract representations for each element, and (b) to score a set after pooling representations of its elements.

**Baselines** We compare to several baselines: (a) **Random** picks a word from the vocabulary uniformly at random. (b) **Bayes Set** (Ghahramani & Heller, 2005b), and (c) **w2v-Near** that computes the nearest neighbors in the word2vec (Mikolov

<sup>5</sup>[github.com/dmlc/experimental-lda](https://github.com/dmlc/experimental-lda)

et al., 2013) space. Note that both Bayes Set and w2v NN are strong baselines. The former runs Bayesian inference using Beta-Binomial conjugate pair, while the latter uses the powerful 300 dimensional word2vec trained on the billion word GoogleNews corpus<sup>6</sup>. (d) **NN-max** uses a similar architecture as our Deepsets with an important difference. It uses max pooling to compute the set feature, as opposed to Deepsets which uses sum pooling. (e) **NN-max-con** uses max pooling on set elements but concatenates this pooled representation with that of query for a final set feature. (f) **NN-sum-con** is similar to NN-max-con but uses sum pooling followed by concatenation with query representation.

**Evaluation** To quantitatively evaluate, we consider the standard retrieval metrics – recall@K, median rank and mean reciprocal rank. To elaborate, recall@K measures the number of true labels that were recovered in the top K retrieved words. We use three values of  $K = \{10, 100, 1k\}$ . The other two metrics, as the names suggest, are the median and mean of reciprocals of the true label ranks, respectively. Each dataset is split into TRAIN (80%), VAL (10%) and TEST (10%). We learn models using TRAIN and evaluate on TEST, while VAL is used for hyperparameter selection and early stopping.

**Results and Observations** Tab. 3 contains the results for the text concept set retrieval on LDA-1k, LDA-3k, and LDA-5k datasets. We summarize our findings below: (a) Our Deepsets model outperforms all other approaches on LDA-3k and LDA-5k by any metric, highlighting the significance of permutation invariance property. For instance, Deepsets is better than the w2v-Near baseline by 1.5% in Recall@10 on LDA-5k. (b) On LDA-1k, neural network based models do not perform well when compared to w2v-Near. We hypothesize that this is due to small size of the dataset insufficient to train a high capacity neural network, while w2v-Near has been trained on a billion word corpus. Nevertheless, our approach comes the closest to w2v-Near amongst other approaches, and is only 0.5% lower by Recall@10.

Topic 1	Topic 2	Topic 3	Topic 4	Topic 5	Topic 6
legend	president	plan	newspaper	round	point
airy	vice	proposed	daily	teams	angle
tale	served	plans	paper	final	axis
witch	office	proposal	news	played	plane
devil	elected	planning	press	redirect	direction
giant	secretary	approved	published	won	distance
story	presidency	planned	newspapers	competition	surface
folklore	presidential	development	editor	tournament	curve

Figure 6. Examples from our LDA-1k datasets. Notice that each of these are latent topics of LDA and hence are semantically similar.

## C. Image Tagging

We next experiment with image tagging, where the task is to retrieve all relevant tags corresponding to an image. Images usually have only a subset of relevant tags, therefore predicting other tags can help enrich information that can further be leveraged in a downstream supervised task. In our setup, we learn to predict tags by conditioning Deepsets on the image. Specifically, we train by learning to predict a partial set of tags from the image and remaining tags. At test time, we the test image is used to predict relevant tags.

**Datasets** We report results on the following three datasets:

(a) *ESPgame* (Von Ahn & Dabbish, 2004): Contains around 20k images spanning logos, drawings, and personal photos, collected interactively as part of a game. There are a total of 268 unique tags, with each image having 4.6 tags on average and a maximum of 15 tags.

(b) *IAPRTC-12.5* (Grubinger, 2007): Comprises of around 20k images including pictures of different sports and actions, photographs of people, animals, cities, landscapes, and many other aspects of contemporary life. A total of 291 unique tags have been extracted from captions for the images. For the above two datasets, train/test splits are similar to those used in previous works (Guillaumin et al., 2009; Chen et al., 2013).

(c) *COCO-Tag*: We also construct a dataset in-house, based on MSCOCO dataset (Lin et al., 2014). COCO is a large image dataset containing around 80k train and 40k test images, along with five caption annotations. We extract tags by first running a standard spell checker<sup>7</sup> and lemmatizing these captions. Stopwords and numbers are removed from the set of extracted tags. Each image has 15.9 tags on an average and a maximum of 46 tags. We show examples of image tags from COCO-Tag in Fig. 7. The advantages of using COCO-Tag are three fold—richer concepts, larger vocabulary and more tags per image, making this an ideal dataset to learn image tagging using Deepsets.

<sup>6</sup>[code.google.com/archive/p/word2vec/](http://code.google.com/archive/p/word2vec/)

<sup>7</sup><http://hunspell.github.io/>

**Image and Word Embeddings** Our models use features extracted from Resnet, which is the state-of-the-art convolutional neural network (CNN) on ImageNet 1000 categories dataset using the publicly available 152-layer pretrained model<sup>8</sup>. To represent words, we jointly learn embeddings with the rest of Deepsets neural network for ESPgame and IAPRTC-12.5 datasets. But for COCO-Tag, we bootstrap from 300 dimensional word2vec embeddings<sup>9</sup> as the vocabulary for COCO-Tag is significantly larger than both ESPgame and IAPRTC-12.5 (13k vs 0.3k).

**Methods** The setup for Deepsets to tag images is similar to that described in Appendix B. The only difference being the conditioning on the image features, which is concatenated with the set feature obtained from pooling individual element representations. The resulting feature forms the new input to a neural network used to score the set, in this case, score the relevance of a tag to the image.

**Baselines** We perform comparisons against several baselines, previously reported from (Chen et al., 2013). Specifically, we have Least Sq., a ridge regression model, MBRM (Feng et al., 2004), JEC (Makadia et al., 2008) and FastTag (Chen et al., 2013). Note that these methods do not use deep features for images, which could lead to an unfair comparison. As there is no publicly available code for MBRM and JEC, we cannot get performances of these models with Resnet extracted features. However, we report results with deep features for FastTag and Least Sq., using code made available by the authors<sup>10</sup>.

**Evaluation** For ESPgame and IAPRTC-12.5, we follow the evaluation metrics as in (Guillaumin et al., 2009) – precision (P), recall (R), F1 score (F1) and number of tags with non-zero recall (N+). Note that these metrics are evaluate for each tag and the mean is reported. We refer to (Guillaumin et al., 2009) for further details. For COCO-Tag, however, we use recall@K for three values of  $K = \{10, 100, 1000\}$ , along with median rank and mean reciprocal rank (see evaluation in Appendix B for metric details).

**Results and Observations** Tab. 4 contains the results of image tagging on ESPgame and IAPRTC-12.5, and Tab. 5 on COCO-Tag. Here are the key observations from Tab. 4: (a) The performance of Deepsets is comparable to the best of other approaches on all metrics but precision. (b) Our recall beats the best approach by 2% in ESPgame. On further investigation, we found that Deepsets retrieves more relevant tags, which are not present in list of ground truth tags due to a limited 5 tag annotation. Thus, this takes a toll on precision while gaining on recall, yet yielding improvement in F1. On the larger and richer COCO-Tag, we see that Deepsets approach outperforms other methods comprehensively, as expected. We show qualitative examples in Fig. 7.

We present examples of our in-house tagging datasets, COCO-Tag in Fig. 7.

## D. Improved Red-shift Estimation Using Clustering Information

An important regression problem in cosmology is to estimate the red-shift of galaxies, corresponding to their age as well as their distance from us (Binney & Merrifield, 1998). Two common types of observation for distant galaxies include a) photometric and b) spectroscopic observations, where the latter can produce more accurate red-shift estimates.

One way to estimate the red-shift from photometric observations is using a regression model (Connolly et al., 1995). We use a multi-layer Perceptron for this purpose and use the more accurate spectroscopic red-shift estimates as the ground-truth. As another baseline, we have a photometric redshift estimate that is provided by the catalogue and uses various observations (including clustering information) to estimate individual galaxy-red-shift. Our objective is to use clustering information of the galaxies to improve our red-shift prediction using the multi-layer Preceptron.

Note that the prediction for each galaxy does not change by permuting the members of the galaxy cluster. Therefore, we can treat each galaxy cluster as a “set” and use permutation-equivariant layer to estimate the individual galaxy red-shifts.

For each galaxy, we have 17 photometric features<sup>11</sup> from the redMaPPer galaxy cluster catalog (Roza & Rykoff, 2014), which contains photometric readings for 26,111 red galaxy clusters. In this task in contrast to the previous ones, sets have different cardinalities; each galaxy-cluster in this catalog has between  $\sim 20 - 300$  galaxies – *i.e.*  $\mathbf{x} \in \mathbb{R}^{N(c) \times 17}$ , where  $N(c)$  is the cluster-size. See 8(a) for distribution of cluster sizes. The catalog also provides accurate spectroscopic red-shift estimates for a *subset* of these galaxies as well as photometric estimates that uses clustering information. 8(b) reports the distribution of available spectroscopic red-shift estimates per cluster.

We randomly split the data into 90% training and 10% test clusters, and use the following simple architecture for semi-

<sup>8</sup>[github.com/facebook/fb.resnet.torch](https://github.com/facebook/fb.resnet.torch)

<sup>9</sup><https://code.google.com/p/word2vec/>

<sup>10</sup><http://www.cse.wustl.edu/~mchen/>

<sup>11</sup>We have a single measurement for each u,g,r, i and z band as well as measurement error bars, location of the galaxy in the sky, as well as the probability of each galaxy being the cluster center. We do not include the information regarding the richness estimates of the clusters from the catalog, for any of the methods, so that baseline multi-layer Preceptron is blind to the clusters.

Table 6. Classification accuracy and the (size of) representation used by different methods on the ModelNet40 dataset.

model	instance size	representation	accuracy
set-layer + transformation (ours)	$5000 \times 3$	point-cloud	$90 \pm .3\%$
set-layer (ours)	$1000 \times 3$	point-cloud	$87 \pm 1\%$
set-pooling only (ours)	$1000 \times 3$	point-cloud	$83 \pm 1\%$
set-layer (ours)	$100 \times 3$	point-cloud	$82 \pm 2\%$
KNN graph-convolution (ours)	$1000 \times (3 + 8)$	directed 8-regular graph	$58 \pm 2\%$
3DShapeNets (Wu et al., 2015)	$30^3$	voxels (using convolutional deep belief net)	77%
DeepPano (Shi et al., 2015)	$64 \times 160$	panoramic image (2D CNN + angle-pooling)	77.64%
VoxNet (Maturana & Scherer, 2015)	$32^3$	voxels (voxels from point-cloud + 3D CNN)	83.10%
MVCNN (Su et al., 2015)	$164 \times 164 \times 12$	multi-view images (2D CNN + view-pooling)	90.1%
VRN Ensemble (Brock et al., 2016)	$32^3$	voxels (3D CNN, variational autoencoder)	95.54%
3D GAN (Wu et al., 2016)	$64^3$	voxels (3D CNN, generative adversarial training)	83.3%

supervised learning. We use four permutation-equivariant layers with 128, 128, 128 and 1 output channels respectively, where the output of the last layer is used as red-shift estimate. The squared loss of the prediction for available spectroscopic red-shifts is minimized.<sup>12</sup> 8(c) shows the agreement of our estimates with spectroscopic readings on the galaxies in the test-set with spectroscopic readings. The figure also compares the photometric estimates provided by the catalogue (see Rozo & Rykoff, 2014), to the ground-truth. As it is customary in cosmology literature, we report the average scatter  $\frac{|z_{\text{spec}} - z|}{1 + z_{\text{spec}}}$ , where  $z_{\text{spec}}$  is the accurate spectroscopic measurement and  $z$  is a photometric estimate. The average scatter using **our model** is .023 compared to the scatter of .025 in the **original photometric estimates** for the redMaPPer catalog. Both of these values are averaged over all the galaxies with spectroscopic measurements in the test-set.

We repeat this experiment, replacing the permutation-equivariant layers with fully connected layers (with the same number of parameters) and only use the individual galaxies with available spectroscopic estimate for training. The resulting average scatter for **multi-layer Perceptron** is .026, demonstrating that using clustering information indeed improves photometric red-shift estimates.

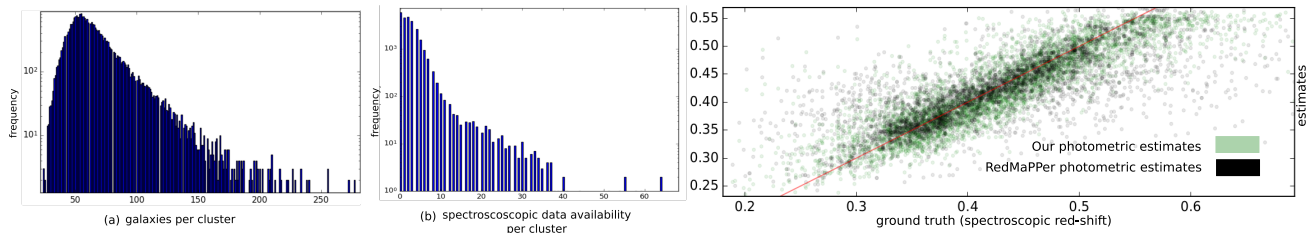


Figure 8. application of permutation-equivariant layer to semi-supervised red-shift prediction using clustering information: **a)** distribution of cluster (set) size; **b)** distribution of reliable red-shift estimates per cluster; **c)** prediction of red-shift on test-set (versus ground-truth) using clustering information as well as RedMaPPer photometric estimates (also using clustering information).

## E. Point Cloud Classification

A low-dimensional point-cloud is a set of low-dimensional vectors. This type of data is frequently encountered in various applications from robotics and vision to cosmology. In these applications, point-cloud data is often converted to voxel or mesh representation at a preprocessing step (e.g. Maturana & Scherer, 2015; Ravanbakhsh et al., 2016b; Lin et al., 2004). Since the output of many range sensors such as LiDAR – which are extensively used in applications such as autonomous vehicles – is in the form of point-cloud, direct application of deep learning methods to point-cloud is highly desirable. Moreover, when working with point-clouds rather than voxelized 3D objects, it is easy to apply transformations such as rotation and translation as differentiable layers at low cost.

Here, we show that treating the point-cloud data as a set, we can use the set-equivariant layer to classify point-cloud representation of a subset of ShapeNet objects (Chang et al., 2015), called ModelNet40 (Wu et al., 2015). This subset

<sup>12</sup>We use mini-batches of size 128, Adam (Kingma & Ba, 2014), with learning rate of .001,  $\beta_1 = .9$  and  $\beta_2 = .999$ . All layers except for the last layer use Tanh units and simultaneous dropout with 50% dropout rate.

consists of 3D representation of 9,843 training and 2,468 test instances belonging to 40 classes of objects; see 9. We produce point-clouds with 100, 1000 and 5000 particles each ( $x, y, z$ -coordinates) from the mesh representation of objects using the point-cloud-library’s sampling routine (Rusu & Cousins, 2011). Each set is normalized by the initial layer of the deep network to have zero mean (along individual axes) and unit (global) variance. Additionally we experiment with the K-nearest neighbor graph of each point-cloud and report the results using graph-convolution.

**Set convolution.** We use a network comprising of 3 permutation-equivariant layers with 256 channels followed by max-pooling over the set structure. The resulting vector representation of the set is then fed to a fully connected layer with 256 units followed by a 40-way softmax unit. We use Tanh activation at all layers and dropout on the layers after set-max-pooling (*i.e.* two dropout operations) with 50% dropout rate. Applying dropout to permutation-equivariant layers for point-cloud data deteriorated the performance. We observed that using different types of permutation-equivariant layers (see Sec. 2.3) and as few as 64 channels for set layers changes the result by less than 5% in classification accuracy.

For the setting with 5000 particles, we increase the number of units to 512 in all layers and randomly rotate the input around the  $z$ -axis. We also randomly scale the point-cloud by  $s \sim \mathcal{U}(.8, 1./ .8)$ . For this setting only, we use Adamax (Kingma & Ba, 2014) instead of Adam and reduce learning rate from .001 to .0005.

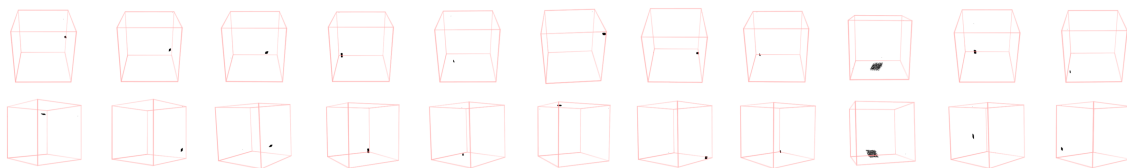
**Graph convolution.** For each point-cloud instance with 1000 particles, we build a sparse K-nearest neighbor graph and use the three point coordinates as input features. We normalized all graphs at the preprocessing step. For direct comparison with set layer, we use the exact architecture of 3 graph-convolution layer followed by set-pooling (global graph pooling) and dense layer with 256 units. We use exponential linear activation function instead of Tanh as it performs better for graphs. Due to over-fitting, we use a heavy dropout of 50% after graph-convolution and dense layers. Similar to dropout for sets, all the randomly selected features are simultaneously dropped across the graph nodes. We use a mini-batch size of 64 and Adam for optimization where the learning rate is .001 (the same as that of permutation-equivariant counter-part).

Despite our efficient sparse implementation using Tensorflow, graph-convolution is significantly slower than the set layer. This prevented a thorough search for hyper-parameters and it is quite possible that better hyper-parameter tuning would improve the results that we report here.

6 compares our method against the competition.<sup>13</sup> Note that we achieve our best accuracy using  $5000 \times 3$  dimensional representation of each object, which is much smaller than most other methods. All other techniques use either voxelization or multiple view of the 3D object for classification. Interestingly, variations of view/angle-pooling (*e.g.* Su et al., 2015; Shi et al., 2015) can be interpreted as set-pooling where the class-label is invariant to permutation of different views. The results also shows that using fully-connected layers with set-pooling alone (without max-normalization over the set) works relatively well.

We see that reducing the number of particles to only 100, still produces comparatively good results. Using graph-convolution is computationally more challenging and produces inferior results in this setting. The results using 5000 particles is also invariant to small changes in scale and rotation around the  $z$ -axis.

Units of the **first** permutation-invariant layer



Units of the **second** permutation-invariant layer

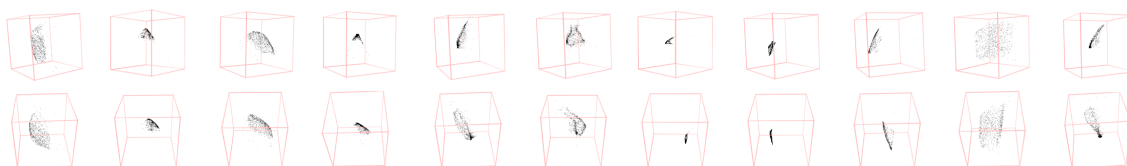


Figure 10. Each box is the particle-cloud maximizing the activation of a unit at the first (**top**) and second (**bottom**) permutation-equivariant layers of our model. Two images of the same column are two different views of the same point-cloud.

<sup>13</sup>The error-bar on our results is due to variations depending on the choice of particles during test time and it is estimated over three trials.



**Features.** To visualize the features learned by the set layers, we used Adamax (Kingma & Ba, 2014) to locate 1000 particle coordinates maximizing the activation of each unit.<sup>14</sup> Activating the tanh units beyond the second layer proved to be difficult. 10 shows the particle-cloud-features learned at the first and second layers of our deep network. We observed that the first layer learns simple localized (often cubic) point-clouds at different  $(x, y, z)$  locations, while the second layer learns more complex surfaces with different scales and orientations.

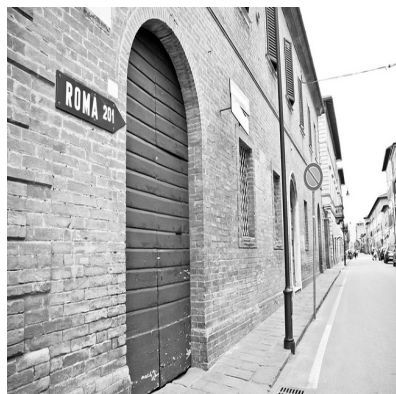
## F. Set Anomaly Detection

The objective here is for the deep model to find the anomalous face in each set, simply by observing examples and without any access to the attribute values. CelebA dataset (Liu et al., 2015) contains 202,599 face images, each annotated with 40 boolean attributes. We use  $64 \times 64$  stamps and using these attributes we build 18,000 sets, each containing  $N = 16$  images (on the training set) as follows: after randomly selecting two attributes, we draw 15 images where those attributes are present and a single image where both attributes are absent. Using a similar procedure we build sets on the test images. No individual person’s face appears in both train and test sets.

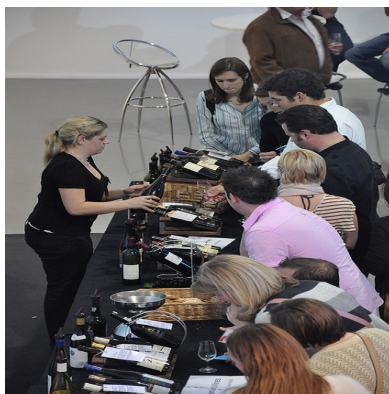
Our deep neural network consists of 9 2D-convolution and max-pooling layers followed by 3 permutation-equivariant layers and finally a softmax layer that assigns a probability value to each set member (Note that one could identify arbitrary number of outliers using a sigmoid activation at the output.) Our trained model successfully finds the anomalous face in **75% of test sets**. Visually inspecting these instances suggests that the task is non-trivial even for humans; see 5. Details of the model, training and more identification examples see below.

As a *baseline*, we repeat the same experiment by using a set-pooling layer after convolution layers, and replacing the permutation-equivariant layers with fully connected layers, with the same number of hidden units/output-channels, where the final layer is a 16-way softmax. The resulting network shares the convolution filters for all instances within all sets, however the input to the softmax is not equivariant to the permutation of input images. Permutation equivariance seems to be crucial here as the baseline model achieves a training and **test accuracy of  $\sim 6.3\%$** ; the same as random selection. Our model has 9 convolution layers with  $3 \times 3$  receptive fields. The model has convolution layers with 32, 32, 64 feature-maps followed by max-pooling followed by 2D convolution layers with 64, 64, 128 feature-maps followed by another max-pooling layer. The final set of convolution layers have 128, 128, 256 feature-maps, followed by a max-pooling layer with pool-size of 5 that reduces the output dimension to batch – size.  $N \times 256$ , where the set-size  $N = 16$ . This is then forwarded to three permutation-equivariant layers with 256, 128 and 1 output channels. The output of final layer is fed to the Softmax, to identify the outlier. We use exponential linear units (Clevert et al., 2015), drop out with 20% dropout rate at convolutional layers and 50% dropout rate at the first two set layers. When applied to set layers, the selected feature (channel) is simultaneously dropped in all the set members of that particular set. We use Adam (Kingma & Ba, 2014) for optimization and use batch-normalization only in the convolutional layers. We use mini-batches of 8 sets, for a total of 128 images per batch.

<sup>14</sup>We started from uniformly distributed set of particles and used a learning rate of .01 for Adamax, with first and second order moment of .1 and .9 respectively. We optimized the input in  $10^5$  iterations. The results of 10 are limited to instances where tanh units were successfully activated. Since the input at the first layer of our deep network is normalized to have a zero mean and unit standard deviation, we do not need to constrain the input while maximizing unit’s activation.



GT	Pred
building	building
sign	street
brick	city
picture	brick
empty	sidewalk
white	side
black	pole
street	white
image	stone



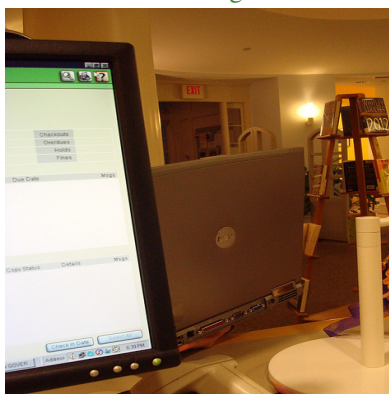
GT	Pred
standing	person
surround	group
woman	man
crowd	table
wine	sit
person	room
group	woman
table	couple
bottle	gather



GT	Pred
traffic	clock
city	tower
building	sky
tall	building
large	tall
tower	large
European	cloudy
front	front
clock	city



GT	Pred
photograph	ski
snowboarder	snow
snow	slope
glide	person
hill	snowy
show	hill
person	man
slope	skiing
young	skier



GT	Pred
laptop	refrigerator
person	fridge
screen	room
room	magnet
desk	cabinet
living	kitchen
counter	shelf
computer	wall
monitor	counter



GT	Pred
beach	jet
shoreline	airplane
stand	propeller
walk	ocean
sand	plane
lifeguard	water
white	body
person	person
surfboard	sky

Figure 7. Qualitative examples of image tagging using Deepsets. *Top row*: Positive examples where most of the retrieved tags are present in the ground truth (brown) or are relevant but not present in the ground truth (green). *Bottom row*: Few failure cases with irrelevant/wrong tags (red). From left to right, (i) Confusion between snowboarding and skiing, (ii) Confusion between back of laptop and refrigerator due to which other tags are kitchen-related, (iii) Hallucination of airplane due to similar shape of surfboard.

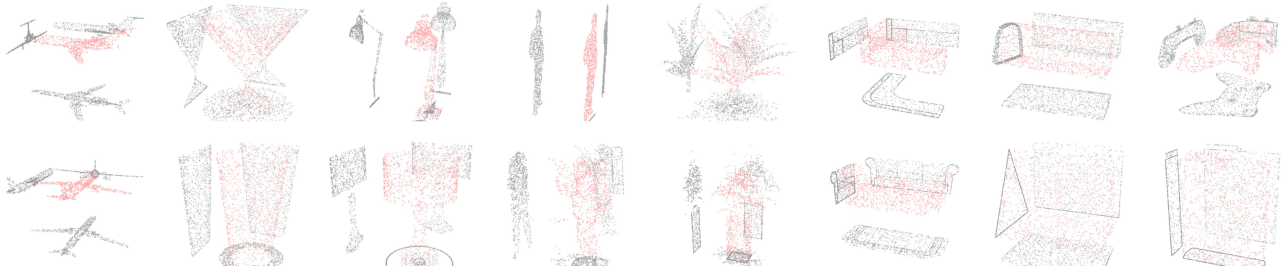


Figure 9. Examples for 8 out of 40 object classes (column) in the ModelNet40. Each point-cloud is produced by sampling 1000 particles from the mesh representation of the original ModelNet40 instances. Two point-clouds in the same column are from the same class. The projection of particles into  $xy$ ,  $zy$  and  $xz$  planes are added for better visualization.



Figure 11. Each row shows a set, constructed from CelebA dataset, such that all set members except for an outlier, share at least two attributes (on the right). The outlier is identified with a red frame. The model is trained by observing examples of sets and their anomalous members, *without access to the attributes*. The probability assigned to each member by the outlier detection network is visualized using a red bar at the bottom of each image.



Figure 12. Each row of the images shows a set, constructed from CelebA dataset images, such that all set members except for an outlier, share at least two attributes. The outlier is identified with a red frame. The model is trained by observing examples of sets and their anomalous members and *without access to the attributes*. The probability assigned to each member by the outlier detection network is visualized using a red bar at the bottom of each image. The probabilities in each row sum to one.